coatings

MDPI

Article

Albumin–Rutin Nanoparticles: Design, Characterization, and Biophysical Evaluation

Claudia G. Chilom [1,*], Adriana Elena Balan [1], Teodor Adrian Enache [2], Daniela Oprea [1,2], Monica Enculescu [2], Monica Florescu [3] and Melinda David [4]

[1] Faculty of Physics, University of Bucharest Magurele, 077125 Magurele, Romania; adriana.balan@unibuc.ro (A.E.B.); daniela.oprea@infim.ro (D.O.)
[2] National Institute of Materials Physics, 077125 Magurele, Romania; adrian.enache@infim.ro (T.A.E.); mdatcu@infim.ro (M.E.)
[3] Faculty of Medicine, Transilvania University of Brasov, 500039 Brasov, Romania; florescum@unitbv.ro
[4] Faculty of Electrical Engineering and Computer Science, Transilvania University of Brasov, 500039 Brasov, Romania; melinda.david@unitbv.ro
* Correspondence: claudia-gabriela.chilom@unibuc.ro

Abstract: The bioavailability of the administered drugs that reach the systemic circulation is the first point in resolving the pathology of patients. Albumin-based nanoparticles represent an increasingly used strategy to deliver cancer drugs into cells that otherwise cannot overcome biological barriers. In this work, rutin (Ru), a flavonoid with anticancer and antioxidant potential, was incorporated into bovine serum albumin nanoparticles (BSA-Ru NPs), developed using the desolvation method, and the entire system was characterized and evaluated by scanning electron microscopy (SEM), atomic force microscopy (AFM), and UV–Vis absorption spectroscopy. The results showed that BSA and BSA–Ru NPs are uniformly distributed, have relatively large sizes, and have a time stability of more than 60%. Furthermore, the effect of these nanohybrids on the thermal stability of liposomal membranes was evaluated by surface plasmon resonance (SPR), cyclic voltammetry (CV), and electrochemical impedance spectroscopy (EIS). The viability evaluation was assessed by the tetrazolium salt (3-(4,5-dimethylthiazol-2-yl)-5-(3-carboxymethoxyphenyl)-2-(4-sulfophenyl)-2H-tetrazolium) (MTS) protocol in the fibroblast L929 line and a high level of biocompatibility, confirmed by SEM results, was found.

Keywords: bovine serum albumin; rutin; nanoparticles; biohybrid; drug delivery

Citation: Chilom, C.G.; Balan, A.E.; Enache, T.A.; Oprea, D.; Enculescu, M.; Florescu, M.; David, M. Albumin–Rutin Nanoparticles: Design, Characterization, and Biophysical Evaluation. *Coatings* **2024**, *14*, 220. https://doi.org/10.3390/coatings14020220

Academic Editor: Giuseppina Raffaini

Received: 20 January 2024
Revised: 5 February 2024
Accepted: 7 February 2024
Published: 10 February 2024

1. Introduction

Organisms' resistance mechanisms to cancer can be inhibited by various strategies, including the use of nanoparticle drug carriers. In this way, the poor pharmacokinetic profiles of some anticancer agents can be overcome, or the stability of the load and release profiles of some drugs can be improved [1]. Protein nanocarriers, such as serum albumin-based nanoparticles, are preferred for the multiple advantages offered by their properties such as biocompatibility, biodegradability, immunogenicity, and low cytotoxicity [2]. Albumin-based nanotransporters are widely used in anticancer strategies, as they can be passively or actively targeted [3,4], are released in a controlled manner, and can bypass mechanisms of resistance to cancer drugs.

In many studies, bovine serum albumin (BSA) is chosen as a carrier protein, partly because of its structural and functional similarities to human serum albumin (HSA), and partly because of its properties, i.e., the binding and transport of various substances like hormones, drugs, etc. in blood, and the neutralisation of free radicals. BSA is a small and stable protein, used in many studies because of its ability to increase signal in assays, and its low cost of purification from bovine blood. Methods for synthesizing BSA NPs must take into account that certain parameters, such as pH or temperature, must be well-controlled to

ensure that the size and behaviour of the NPs are as desired and allow for the incorporation and release of drugs [5]. In this sense, the desolvation method is very suitable for the synthesis of BSA nanoparticles (NPs) [6,7] because it is simple and allows for the use of different cross-linking agents to optimize the production of NPs [8]. Among them, sugars, such as glucose, increase the conformational stability of proteins [9].

The functional amino and carboxyl groups of BSA provide functionalization of BSA NPs by targeting molecules or molecules with therapeutic activity [10]. One of these molecules is rutin (Ru), a flavonoid that is found in vegetables and fruits and exhibits strong antioxidant and anticancer activities [11], but has the disadvantage that it is not soluble in aqueous solvents and shows poor stability over time. These aspects limit the use of Ru in medical applications. Some studies show that Ru has anticarcinogenic potential, inhibiting the proliferation (via apoptotic induction) of several types of cancer cells [12]). One way to improve the stability of Ru could be to create hybrid structures with proteins such as serum albumins. In such nanohybrids, Ru can be used in various therapeutic formulations, in which it has improved solubility and efficacy. Although Ru is insoluble in aqueous solvents, it can be used in biological applications through its incorporation into liposomes (biocompatible lipid vesicles capable of transporting hydrophilic, hydrophobic, and amphiphilic molecules) or by covering them with a thin layer. In such nontoxic biohybrids, Ru has a cytotoxic effect and protects cells from oxidative stress [13].

The interest in the use of Ru comes from its protective properties, due to its antioxidant activity, on the one hand, and from the fact that it forms a complex with a relatively high affinity to serum albumin [14,15], on the other hand. In addition, Ru appears to mediate oncogenic pathways in various carcinomas and to modulate, through interaction with mRNA, important cellular functions [12]. The effect of Ru on tumour cells has previously been tested in vitro; the production of tumour necrosis factor-alpha (TNF-alpha) and nitric oxide (NO) by L929 colon tumour cells was inhibited by Ru treatment [16]. Ru, in various experimental formulations, such as hydrogels, has been tested in the treatment of inflammatory intestinal disease, and the results showed an inhibition of overexpressed inflammatory cytokines, including TNF-α and IL-6 [17]. Also, Ru has been shown to be one of the nontoxic flavonoids for human lung embryonic fibroblast (TIG-1) cells and human umbilical vein endothelial cells (HUVE) [18]. Given the ability of some flavonoids to potently inhibit the bacterial efflux pump, the effect of Ru altering the antibiotic resistance of *Staphylococcus aureus* strains was investigated. Cell tests on fibroblast cultures did not show antibiotic potentiation by Ru [19].

Ru inhibits cell proliferation and removes reactive oxygen species. Studies have shown that Ru has chemopreventive action in cancer [20], and Ru treatment significantly reduces lipidic peroxidase [21]. The fact that Ru has enhanced anticancer efficacy through targeted delivery and the sustained release of anticancer drugs makes it a good candidate for studies to design new delivery systems for anticancer agents [22].

Since Ru's solubility in water is very low, various nanotechnological approaches are reported in the literature to enhance the Ru delivery at the cellular level, polymer nanoparticles, or lipid nanoparticles [22]. However, for Ru's effects to be useful in the treatment of various chronic human diseases, Ru's bioavailability must be improved. Therefore, new ways to potentiate Ru's effects at the cellular level are being developed, and one approach is to use Ru in formulations such as protein nanoparticles [23].

The nanoparticles (NPs) preparation method must be adapted to each type of NPs. Serum albumin-based nanoparticles for drug delivery purposes can be prepared by several methods: self-assembly, emulsification, thermal gelation, nano spray drying, and desolvation [24]. The most commonly used is desolvation, due to the possibility of relatively easily adjusting the preparation conditions (pH, ionic strength, amount of desolving agent, concentration of cross-linking agent, and drug content) [25] to obtain the desired size of NPs for various applications.

In the present study, the preparation method for bovine serum albumin–rutin-loaded nanoparticles (BSA–Ru NPs) is described. Furthermore, these NPs are morphologically

characterized, and their effect on liposomal membranes and healthy fibroblast cells, namely L929, was investigated. The results may have an impact on understanding the mechanism of action of protein biohybrids on cells, for biomedical purposes.

2. Experimental

2.1. Materials

Bovine serum albumin (BSA, 66 kDa) and glucose (D-(+)-Glucose, 180.156 Da, ≥99.5%) were purchased from Fisher Scientific (Loughborough, UK). Rutin (Ru, 610.52 Da, 97%) was purchased from Acros Organics (Geel, Belgium). Ethanol (EtOH, 46.07 Da, ≥99.8%), chloroform (119.38 Da, ≥99.5%), and phosphate-buffered saline (PBS, tablets) were purchased from Merck Company (Darmstadt, Germany). Dipalmitoylphosphatidylcholine phospholipid (DPPC, >99%) was purchased from Avanti Polar Lipids (Birmingham, UK).

For biological assays, a fibroblast cell line ATCC CCL-2 male mouse (L929 F10 cell line, Manassas, Virginia, USA) was utilized. All of the following reagents were used as received: Dulbecco's Modified Eagle Medium (DMEM, Thermo Fisher Scientific, Waltham, MA, USA), foetal bovine serum (FBS, Thermo Fisher Scientific, Waltham, MA, USA), phosphate-buffered saline without calcium and magnesium (PBS, Thermo Fisher Scientific, Waltham, MA, USA), 0.25% trypsin/ethylenediaminetetraacetic acid (EDTA) solution (Thermo Fisher Scientific, Waltham, MA, USA), and antibiotics (Biological Industries, Kibbutz Beit-Haemek, Israel). The tetrazolium salt (3-(4,5-dimethylthiazol-2-yl)-5-(3-carboxymethoxyphenyl)-2-(4-sulfophenyl)-2H-tetrazolium) (MTS) kit was purchased from Thermo Fisher Scientific, Waltham, MA, USA and used according to supplier instructions.

The cell growing process was performed in DMEM culture medium, supplemented with 10% foetal bovine serum, 4.5 g/L glucose, 2 mM L-glutamine, penicillin (100 U/mL), and streptomycin (100 µg/mL), in a controlled environment (temperature 37 °C, 5% CO_2 atmosphere). Sub-cultivation was realized in cell culture flasks (T-25 type) when a pre-confluence of cells was achieved of ~80%. For cell fixation, formaldehyde, glutaraldehyde, and osmium tetroxide (Merck, Germany) were used.

2.2. Methods

2.2.1. Preparation of Albumin and Albumin–Rutin-Loaded Nanoparticles

BSA NPs were prepared by desolvation at room temperature, using ethanol as a desolvation agent and glucose as cross-linking agent, following a previously reported method [7]. Briefly, 200 mg/mL BSA was dissolved in distilled water and the solution was brought to pH 8.25. The BSA solution was continuously stirred (550 rpm, CRS 15X CAPP, AHN, Nordhausen, Biotechnologie GMbH, Germany) at room temperature (25 °C) and a volume of 8 mL of pure EtOH 96% was added dropwise (1 mL/min), until the suspension became cloudy. Afterwards, the suspension was centrifuged three times (10,000× *g*, for 10 min), with each centrifugation being followed by ultrasonication in an ultrasound bath (BRANSON 1210, Marshall Scientific, Boston, USA) for 5 min. After each centrifugation, the suspension was resuspended in the same volume of distilled water. For the preparation of BSA–Ru NPs, the same protocol was followed, using a ratio of BSA–Ru of 1:5 (*w*/*w*).

2.2.2. Preparation of *Dipalmitoylphosphatidylcholine* (DPPC) Liposomes and *Dipalmitoylphosphatidylcholine* (DPPC)/Bovine Serum Albumin (BSA)–Rutin Biohybrids

BSA–Ru NPs were diluted to a concentration of 0.5 mM in 10 mM PBS, pH 7.9 (tablets) (equivalent to 300 µL NPs in 3 mL NaPBS). DPPC liposomes were prepared using an already reported protocol [26]. Briefly, DPPC phospholipids were dissolved in chloroform at a concentration of 50 mM, homogenized, and left to evaporate. After evaporation, 3 mL 10 mM PBS was added to the thin lipid film in order to obtain the DPPC liposomes. For the DPPC biohybrids, 3 mL of the previously obtained 0.5 mM BSA–Ru NPs solution was added. To initiate the process of liposome formation for the two systems (DPPC and DPPC/BSA–Ru NPs), the tubes were placed in a water bath at 45 °C for 5 min, and then vortexed for about 10 s. This process was repeated three times, after which the samples

were introduced in an ultrasound bath for 15 min (45 °C). In the end, the samples were allowed to cool to the ambient temperature and then kept at 4 °C for 24 h to ensure complete lipid hydration and balance the liposomal system with the NPs.

2.2.3. Viability Assay

For the viability assay, the L929 cells were plated in 96-well plates at a density of 10,000 cells/well and placed in the incubator at 37 °C for 24 h. After the incubation, the medium was renewed and the nanoparticles added at different concentrations, from 0.2 to 2 mg mL^{-1}, and incubated for 24 h. Following the second incubation, the medium was replaced again and 10 µL MTS solution was added to each well. After 4 h, the absorption at 490 nm was recorded using a plate reader FLUOstar Omega, BMG Labtech, Ortenberg Germany.

2.2.4. Cell Fixation

For the field emission scanning electron microscopy (FESEM) assay, the L929 cells were seeded on a biocompatible glass strip. Following 48 h incubation, of which 24 h was with 1 mg mL^{-1} NP treatment, the cell cultures were washed with PBS and fixed for 10 min with 3% formaldehyde and 0.2% glutaraldehyde. In order to avoid the polarization and the damage of the sample under an electron beam, a 20 min post-fixation, using 0.2% OsO_4 (osmium tetraoxide), was necessary. The OsO_4 treatment was preferred to any metal coating that could interfere with the surface of the cells.

2.3. Instrumentation

2.3.1. Atomic Force Microscopy (AFM)

The 3D topography and phase contrast images for BSA–Ru NPs were obtained using SPM-NTegra Prima AFM (NT-MDT, Moscow, Russia) equipment operated in semi-contact mode. A NSG 01 cantilever, with a resonance frequency between 87 kHz and 230 kHz and constant force between 1.45 N m^{-1} and 15.1 N m^{-1}, was used. Samples were deposited on freshly cleaned mica and dried at room temperature.

2.3.2. Scanning Electron Microscopy (SEM)

The morphology of the samples was investigated using a Gemini 500 Carl Zeiss field emission scanning electron microscope (FESEM) working in both high vacuum (HV) and variable pressure (VP) modes, from 0.2 to 30 kV, equipped with InLens and SE2 detectors.

2.3.3. Ultraviolet–Visible Light Absorption Spectroscopy

A double-beam Perkin Elmer Lambda 750 UV–Vis spectrophotometer (Waltham, MA, USA) was used for the recording of the UV–Vis absorption spectra. Spectra were collected at room temperature, in the wavelength range of 200–800 nm, at a scan speed of 1 nm s^{-1}.

For the cell viability assay, an MTS reagent was added to each sample, and, after 4 h of incubation, the culture medium was collected and the absorption at 490 nm was recorded using a plate reader (FLUOstar Omega, BMG Labtech, Ortenberg, Germany).

2.3.4. Surface Plasmon Resonance

SPR measurements were performed at the flat gold chips (BioNavis LTD, Tampere, Finland) using an MP-SPR NaviTM 200 OTSO instrument. The SPR system was equipped with a thermostat and the measurements were performed in an electrochemical cell with a volume of 100 µL, into which the samples were manually injected. The temperature was varied between 29 and 43 °C, in order to cover the temperature interval where the pre-transition and main transition temperatures of the DPPC lipids occur, since these may affect the interaction of the lipids with the NPs.

2.3.5. Electrochemistry

Cyclic voltammetry (CV) and electrochemical impedance spectroscopy (EIS) measurements were performed using a PalmSens 4 potentiostat (Palm Instruments BV, Houten, The Netherlands). The potentiostat was connected to the electrochemical cell of the SPR equipment, with the gold chip (BioNavis LTD, Finland) considered as the working electrode, and Ag wires as the counter and reference electrodes. Using CV and EIS, the effect of NPs on the liposomes was investigated as a function of temperature for the DPPC biohybrids, compared with the DPPC liposomes. CVs were performed by scanning the working potential between 0.0 and 0.8 V vs. Ag, with a scan rate of 50 mV s^{-1}. The EIS measurement parameters were optimized at a fixed potential of −0.1 V vs. Ag, the frequency being swept between 0.05 and 25 kHz, thus recording the Nyquist spectra. The CV and EIS analyses provided information on interfacial charge transfer and diffusion processes, as well as charge accumulation at the interface, along with dielectric properties and lipidic film thickness, as evidenced by changes in the values of equivalent electrical circuit components obtained by fitting the Nyquist spectra.

3. Results and Discussion

3.1. Morphological Characterization and Stability of Bovine Serum Albumin–Rutin Nanoparticles

The first step in evaluating the NPs obtained by the desolvation method was to characterize their morphology and stability. BSA NPs have already been evaluated in a recent study, by means of AFM and SEM [7].

As can be seen in Figure 1, the AFM technique in the semi-contact mode revealed that the BSA–Ru NPs deposited on a mica substrate had regular shapes (Figure 1A–D) and small sizes (Figure 1E), and a maximum height mean value of 73.76 ± 20.73 nm was estimated using the grain analysis tool of the equipment image analysis software. Particle profiles, which are presented in Figure 1F, had a maximum height in the interval 60–90 nm with a symmetrical shape. There was no evidence of protein aggregates. Comparing with previously obtained results [7], we found that BSA NPs and BSA–Ru NPs had similar morphologies and sizes (below 100 nm), making them suitable for further testing on their effect on various cell lines, as will be seen in Section 3.4.

The previous results obtained by SEM for BSA NPs showed a homogenous population nanosized around 200 nm [7]. The same tendency to form spherical particles was also observed for BSA–Ru NPs (Figure 1G–K). SEM images were recorded to highlight the distribution and morphology of the BSA NPs (Figure 1G) and the BSA–Ru NPs (Figure 1I), and it was observed that BSA NPs showed aggregation tendencies. The images obtained at different magnifications for BSA–Ru NPs deposited on silica strips revealed a uniform dispersal and a lower condensation level than BSA NPs. While BSA NPs tended (Figure 1H) to form large aggregates, the BSA–Ru NPs (Figure 1J) presented a uniform distribution and a low aggregation profile; this is the reason for which, at low magnifications, the BSA–Ru NPs are not observed.

The size distribution measurements showed that BSA–Ru NPs were around 350 nm (Figure 1K). By comparison, their size is larger than previously obtained BSA NPs using the same methodology [7], but comparable to the sizes obtained for BSA NPs in which Ru was incorporated by other methods, e.g., using nano spray drying [27] or the single-emulsion solvent evaporation method [28]. The particles' sizes, as evaluated by SEM, were much larger than those obtained by AFM, probably due to the shrinkage of BSA–Ru NPs during the drying process for AFM imaging. Such results have been reported previously for BSA NPs [29].

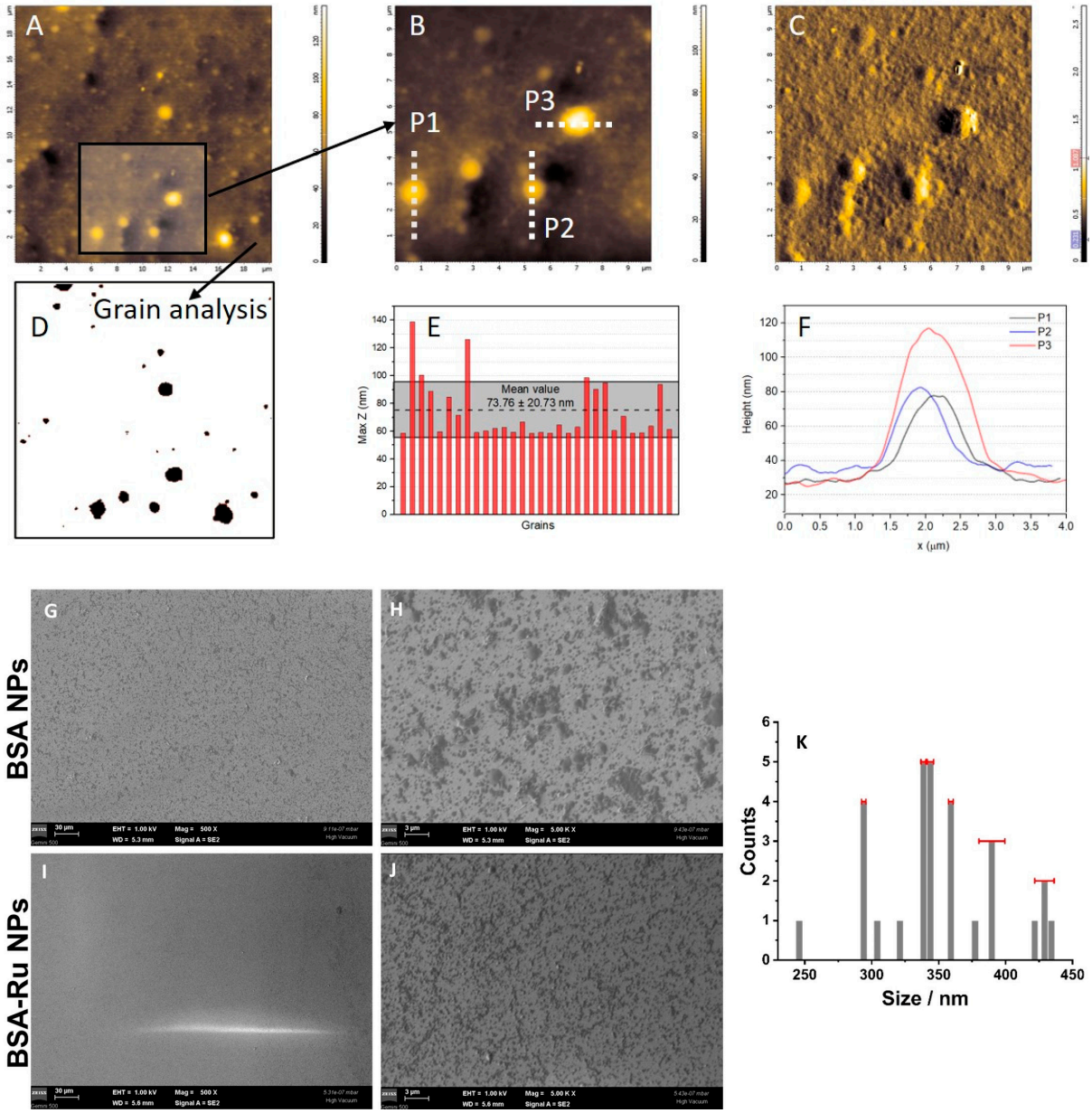

Figure 1. AFM (**A**–**F**) and SEM (**G**–**K**) investigations of BSA–Ru NPs: (**A**) topography AFM image in semi-contact mode on a 20 μm × 20 μm surface; (**B**) topography on a 10 μm × 10 μm surface area; (**C**) phase contrast image corresponding to the image (**B**); (**D**) grain analysis on the image (**A**); (**E**) maximum height histogram of the grains selected in the image (**D**); (**F**) sections P1–P3 in the image (**B**) showing BSA–Ru NPs profiles. SEM images at different magnifications (**G**–**J**) and particles distributions (**K**) obtained for BSA–Ru NPs.

The stability of NPs was assessed by their UV–Vis absorption, recording spectra at different time periods. In order to follow the stability over time of BSA–Ru NPs, UV–Vis spectra were recorded between 200 and 800 nm. The tryptophan (Trp) amino acid-induced changes in BSA structure were investigated over a period of one month by monitoring absorbance at 280 nm. These data were compared with the results previously obtained for BSA NPs [7], as one can see from Figure 2. The BSA–Ru NPs absorbance changed in the first 15 days, after which there were no more significant changes, and the stability over time was 63%, comparable with those for BSA NPs (67%) [7].

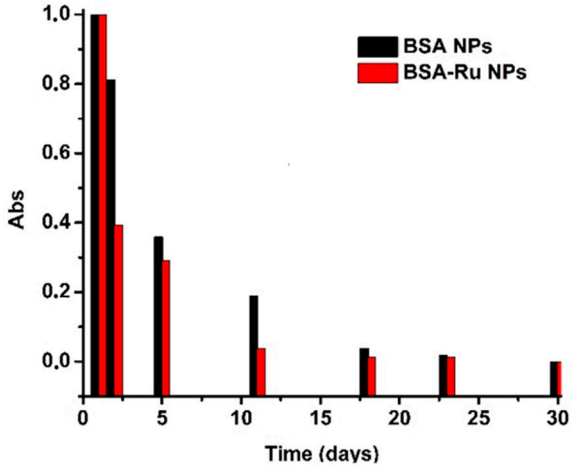

Figure 2. The stability of BSA NPs [7] and BSA-Ru NPs over a period of 30 days.

3.2. Surface Plasmon Resonance Characterization of Dipalmitoylphosphatidylcholine (DPPC) Liposomes and Dipalmitoylphosphatidylcholine (DPPC)/Bovine Serum Albumin (BSA)–Rutin Biohybrids

Biohybrids obtained using non-fluorescent DPPC liposomes, whose preparation was described in Section 2.2.2, were used for SPR measurements. As demonstrated in a previous work [7], the presence of BSA NPs led to a reorganization of the liposome membrane through the interaction between the amino acid functional groups in the BSA NPs and the polar head groups of the lipids. The effect of the BSA–Ru NPs on the DPPC liposomes and the thermal stability of the DPPC biohybrids were determined. Since gold has a hydrophobic character, DPPC liposomes and DPPC biohybrids should be ordered in the vicinity of the sensor surface in the form of a lipid film. DPPC and DPPC/BSA–Ru biohybrids were injected at the 29 °C preheated sensor surface after the stabilization of the signal of the buffer solution. The signal stabilization was achieved before the temperature gradually increased.

Ru acts as a capping agent for the BSA NPs; due to a large number of free -OH groups, it is assumed that the polar lipid groups will preferentially interact with the outer side of the lipidic film and will not allow their penetration into the membrane. This behaviour was confirmed when studying the similarities in temperature dependency and stability of the DPPC and the DPPC/BSA–Ru biohybrid (Figure 3).

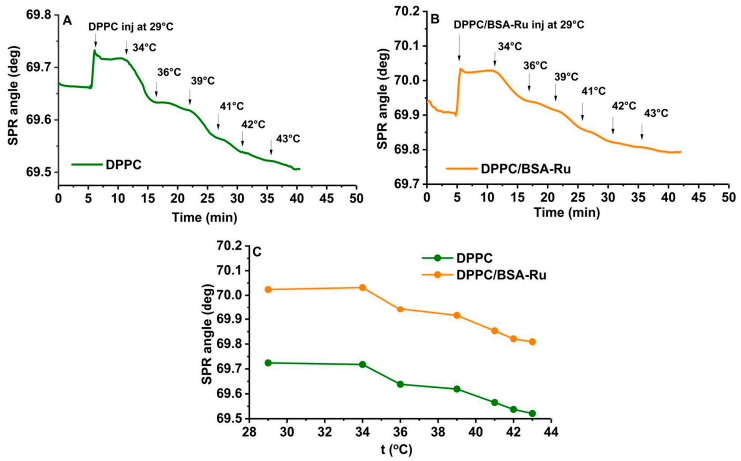

Figure 3. SPR resonance angle variation at different temperatures for (**A**) DPPC, (**B**) DPPC/BSA–Ru biohybrid, and (**C**) temperature dependency for both systems.

3.3. Electrochemical Characterization of Dipalmitoylphosphatidylcholine (DPPC) Liposomes and Dipalmitoylphosphatidylcholine (DPPC)/Bovine Serum Albumin (BSA)–Rutin Biohybrids

3.3.1. Cyclic Voltammetry

The effect of the BSA–Ru NPs in DPPC liposomal systems as a function of temperature was also analysed using electrochemical measurements. Figure 4 shows the CVs of the DPPC liposomes and DPPC biohybrids for a selection of temperatures. For all systems, an increase in the CV width can be noticed, highlighting both the influence of temperature on the membrane fluidity, as well as the interactions between the liposomes and BSA–Ru NPs. The sharp oxidation peak at 0.7 V (Figure 4A) is characteristic of the DPPC liposomes and is more pronounced in the vicinity of the transition temperature (starting with 39 °C). In the case of the DPPC biohybrids (Figure 4B), the intensity of this peak significantly decreases. This is due to the competitive oxidation of the phenolic group present in both tyrosine residue in the BSA NPs and Ru, which occur in the vicinity of 0.7 V [30]. On the reverse scan, a reduction peak occurs at 0.4 V, corresponding to the reduction of the ortho-quinone species formed due to phenol oxidation (catechol-like species). On the following anodic cycles, a new oxidation peak occurs at 0.2 V, concomitant with the anodic charge transfer of the catechol-like species, around 0.4 V. The anodic peak at 0.2 V can be associated with the oxidation product of resorcinol (a hydroquinone species), a moiety of Ru in an electrochemical–chemical mechanism by which the oxidation product is not electroactive [30]. Ru is a well-known antioxidant compound with electrocatalytic behaviour [31], and since it covers the BSA NPs, its reversible behaviour is visible, highlighting that BSA–Ru NPs do not penetrate the liposomal membrane, but rather interact through ionic and van der Waals interactions with the polar head of the lipids.

3.3.2. Electrochemical Impedance

To further highlight the changes induced in the DPPC and DPPC biohybrid systems, EIS measurements were performed in the same temperature range, with a selection of several temperatures (29, 36, and 41 °C) for each system (Figure 4C,D). As a result of fitting the Nyquist spectra, it was possible to highlight the variations in the parameters of the equivalent electrical circuit depending on the temperature (Figure 4E,F) and their correlation with the properties and thermal stability of the systems.

The equivalent electrical circuit (Figure 4E inset) used for the analysis of these spectra was characterized by the resistance of the analysed solution (electrolyte containing DPPC liposomal and biohybrid systems), linked to a parallel combination of the charge transfer resistance (R_{ct}) through the interface and the double layer capacitance (CPE_{dl}) at the Au chip/electrolyte interface. This simple circuit is characteristic of an imperfect capacitor but also appears when modelling the behaviour of an imperfect dielectric, such as the artificial lipid membrane devoid of pores or other defects [32]. Thus, liposomes and biohybrids ordered in the vicinity of the electrode surface as a lipidic film, can be characterized by a non-ideal capacitive element with a frequency-independent negative phase between current and voltage, modelled by a constant phase element (CPE). The impedance of the CPE is $Z_{CPE} = [C(i\omega)^{\alpha}{}_{dl}]^{-1}$, where C is the ideal capacity of CPE parameter in F $s^{\alpha}{}_{dl}{}^{-1}$, ω is the angular frequency, and the α_{dl} exponent reflects the deviation from an ideal capacitor and can reflect the roughness of the lipidic film surface. It can vary between 1.0 for a perfectly smooth surface (ideal capacitor), 0.5 for an uneven surface (highlighting diffusional processes) and 0 describing a pure resistor. In all cases, at 0.05 Hz, the impedance of the system decreases with increasing temperature, enabling a better electron transfer with increasing membrane fluidity.

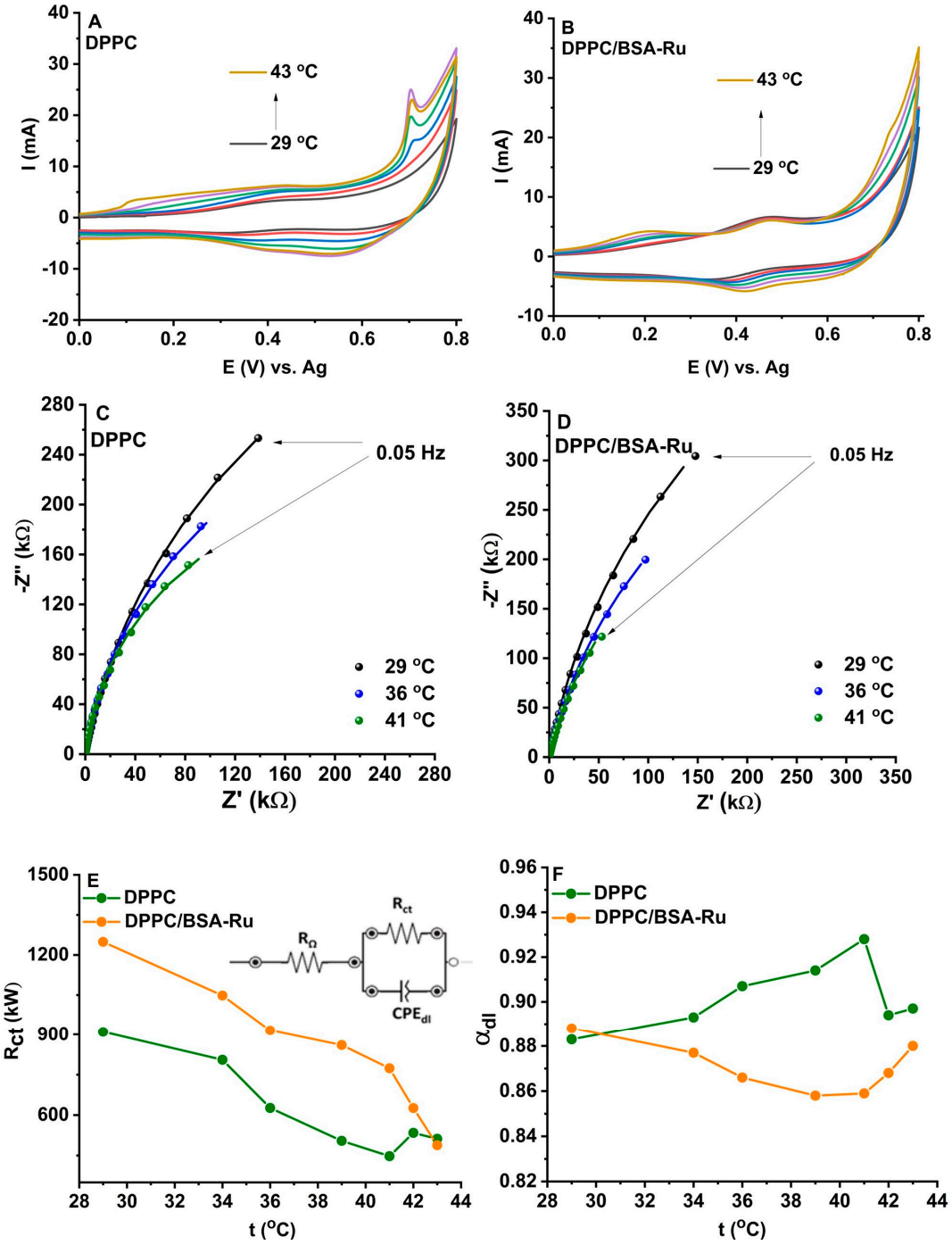

Figure 4. CVs of DPPC (**A**) and DPPC/BSA–Ru NPs (**B**) systems for increasing temperatures. Nyquist spectra of DPPC (**C**) and DPPC/BSA NPs (**D**) systems for increasing temperatures. Electrical equivalent circuit (inset, variation for DPPC, and DPPC/BSA–Ru NPs depending on the temperature of (**E**) R_{ct}, and α_{dl} (**F**).

As the overall impedance of all systems decreases, so does the charge transfer resistance. For the DPPC/BSA–Ru biohybrids, the decrease is continuous, whereas in the case of DPPC liposomes, after the transition temperature an increase can be noticed. However, for both systems, the better electron transfer can be correlated with the SPR angle shift to lower values, which illustrates the increased membrane fluidity and permittivity. Thus, the thickness of the lipidic film decreases and can be correlated with the overall tendency of an increase in α_{dl} values, contributing to the lipidic film homogeneity with increasing

temperature. For the DPPC liposomal system, α_{dl} values continuously increase from 0.883 (29 °C) up to 0.928 (41 °C), after which they abruptly decrease to 0.894. This decrease, however, is not sharp enough to drastically influence the lipidic film homogeneity. For the DPPC/BSA–Ru biohybrids, the presence of NPs stabilizes the behaviour of the lipidic film with increasing temperatures. There is no significant change in α_{dl} values at 29 °C (0.887) and 43 °C (0.879); there is, however, a decrease in the proximity of the pre-transition temperature (0.858—at 39 °C), followed by a drastic increase from 0.859 at 41 °C to 0.880 for 43 °C, associated with the ionic interactions between lipids and NPs. These results agree with the results obtained by cyclic voltammetry.

Throughout the manuscript, we addressed the thermal stability of DPPC biohybrid systems by studying the influence of temperature in the vicinity of human body temperature (36–37 °C). Using both SPR and electrochemical techniques, we observed that the behaviour of the biohybrid system is similar to that of DPPC liposomes. Our measurements show that there is no significant change, which means that our biohybrid system is stable in the chosen thermal range and that the bonds/interactions between lipids and NPs are maintained.

3.4. The Effect of Bovine Serum Albumin–Rutin Nanoparticles at a Cellular Level

To highlight the effect of protein NPs on cells, cell viability tests were performed on L929 mouse fibroblast culture. For these tests, L929 cells were incubated for 24 h with various concentrations (0.2–2.0 mg mL^{-1}) of BSA NPs and rutin-loaded–BSA nanoparticles (BSA–Ru NPs). Cell viability was obtained using the MTS protocol and it was observed that no pronounced cytotoxic effect occurred, with the lowest values of viability obtained being over 85% for BSA NPs and over 75% for BSA–Ru NPs (Figure 5). Such results were also obtained on other types of fibroblasts, as mentioned in the introductory section [18].

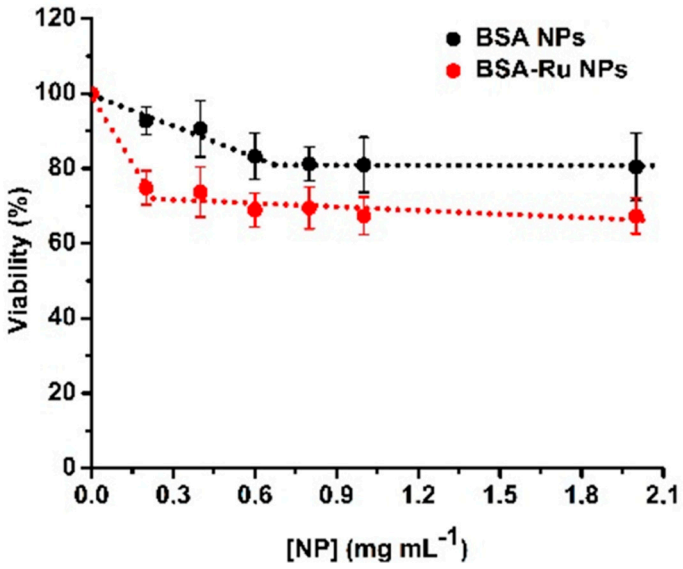

Figure 5. Cell viability of L929 cells in the presence of BSA NPs (black) and BSA-Ru NPs (red).

Also, the interaction between L929 cells and the two types of NPs, BSA NPs and BSA–Ru NPs, was investigated using SEM from a morphological point of view. For this purpose, after 24 h incubation of cell culture with 1 mg mL^{-1} NPs, cells were fixed with 3% paraformaldehyde and 0.25% glutaraldehyde and postfixed with 0.2% osmium tetraoxide. SEM images were also obtained for L929 cells grown on microscope plates, without any additional treatment.

Following the SEM investigation of the interaction between L929 cells and the two types of NPs (Figure 6B1–B3,C1–C3), the typical morphology of fibroblasts was observed when compared with the images taken for the control experiments (Figure 6A1–A3). The

fact that the NPs presented with high biocompatibility for this cell line is highlighted, as no visible toxicity or deformation occurred in L929 cells incubated with the two types of NPs.

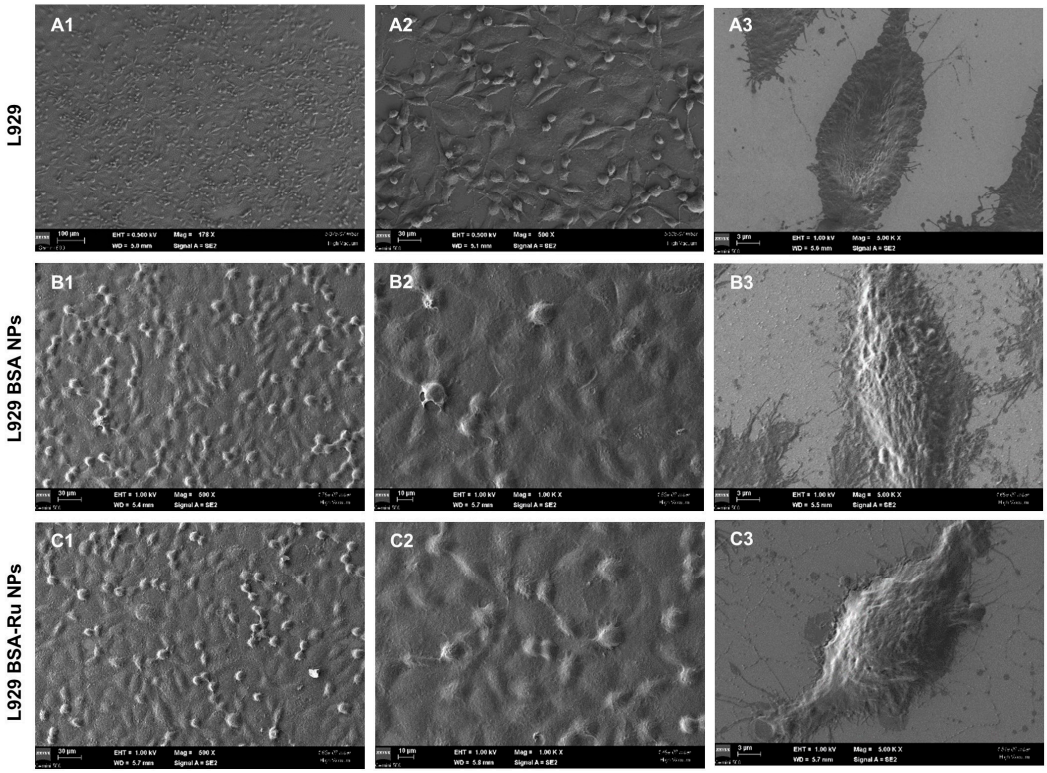

Figure 6. SEM images obtained at different magnifications for control L929 cells (**A1**–**A3**), L929 cells incubated with BSA NPs (**B1**–**B3**), and L929 cells incubated with BSA–Ru NPs (**C1**–**C3**). The magnification of the images was 500× for (**A1**,**B1**,**C1**) samples, 1.00 K× for (**A2**,**B2**,**C2**) and, respectively, 5.00 K× for (**A3**,**B3**,**C3**) samples.

4. Conclusions

The bovine serum albumin nanoparticles, simple and rutin-loaded, were produced by a previously optimized desolvation method to obtain the smallest particle size and most stable nanoparticles during storage, respectively. The desolvation method provided NPs with comparable sizes to those reported in the literature using other methods. Also, this method allowed the solubilization of rutin to be as effective as possible in targeting L929 cells. The stability of the two types of NPs was evaluated for 30 days and was higher than 60%. BSA–Ru NPs were studied morphologically using AFM and SEM, and the results showed that the particles formed were spherical, uniformly distributed on the surface, and of nanometre size.

SPR and electrochemical measurements highlighted the influence induced by the BSA–Ru NPs on the DPPC liposomal system. It was shown that BSA–Ru NPs interacted with the liposomes preferentially in the vicinity of the lipid pre-transition temperature, where they bonded with the lipids polar head groups via ionic and van der Waals interactions, being good candidates for drug delivery systems.

In vitro viability and the morphological modification of L929 cell cultures upon interaction with the NPs were investigated through the MTS assay and SEM microscopy, respectively, and a high level of viability was obtained for both NP systems.

The results obtained in this study, in which multiple spectroscopic and microscopic techniques were used, aimed to visualize the changes in fibroblast cells exposed to BSA nanoparticles loaded with rutin. These results suggest that nanoparticle-based formulations of serum proteins are promising as efficient delivery systems and can be considered a

starting point for future in vitro studies, in which to monitor the cellular response induced by flavonoids and to evaluate their potential therapeutic effects.

Author Contributions: Conceptualization, C.G.C., A.E.B., M.E., M.F. and M.D.; methodology, T.A.E., D.O. and M.E.; validation, C.G.C., A.E.B., T.A.E., M.F. and M.D.; formal analysis, C.G.C., A.E.B., T.A.E., D.O., M.E., M.F. and M.D.; investigation, C.G.C., A.E.B., T.A.E., D.O., M.E., M.F. and M.D.; resources, C.G.C., A.E.B., T.A.E., D.O., M.E., M.F. and M.D.; writing—original draft preparation, C.G.C., A.E.B., T.A.E., M.F. and M.D. All authors have read and agreed to the published version of the manuscript.

Funding: This work was supported by the Project No. 582PED/2022, New hybrid protein nanostructures for targeting specific in colon tumor cells (Prot-Col-Target), PN-III-P2-2.1-PED-2021-1323/01.08.2022. PRO-DD (POS-CCE, O.2.2.1., ID 123, SMIS 2637, No 11/2009) for providing some of the infrastructure used in this work.

Institutional Review Board Statement: Not applicable for studies not involving humans or animals.

Informed Consent Statement: Not applicable.

Data Availability Statement: No new data were created or analyzed in this study. Data sharing is not applicable to this article.

Acknowledgments: CC and AB thank Sorina Iftimie, Faculty of Physics, University of Bucharest, for her help in acquiring UV–Vis absorption spectroscopy data and for all her support in this study. MD and MF thank Arkadiusz Matwijczuk, Department of Biophysics, University of Life Sciences in Lublin, Lublin, Poland for the DPPC lipids and liposomes preparation protocol.

Conflicts of Interest: The authors declare no conflict of interest.

References

1. Hassanin, I.; Elzoghby, A. Albumin-based nanoparticles: A promising strategy to overcome cancer drug resistance. *Cancer Drug Resist.* **2020**, *3*, 930–946. [CrossRef]
2. Verma, D.; Gulati, N.; Kaul, S.; Mukherjee, S.; Nagaich, U. Protein based nanostructures for drug delivery. *J. Pharm.* **2018**, *2018*, 9285854. [CrossRef]
3. Rempel, S.A.; Ge, S.; Gutiérrez, J.A. SPARC: A potential diagnostic marker of invasive meningiomas. *Clin. Cancer Res.* **1999**, *5*, 237–241. [PubMed]
4. Maeda, H.; Wu, J.; Sawa, T.; Matsumura, Y.; Hori, K. Tumor vascular permeability and the EPR effect in macromolecular therapeutics: A review. *J. Control. Release* **2020**, *65*, 271–284. [CrossRef] [PubMed]
5. Bronze-Uhle, E.S.; Costa, B.C.; Ximenes, V.F.; Lisboa-Filho, P.N. Synthetic nanoparticles of bovine serum albumin with entrapped salicylic acid. *Nanotechnol. Sci. Appl.* **2017**, *10*, 11–21. [CrossRef] [PubMed]
6. Jahanban-Esfahlan, A.; Dastmalchi, S.; Davaran, S. A simple improved desolvation method for the rapid preparation of albumin nanoparticles. *Int. J. Biol. Macromol.* **2016**, *91*, 703–709. [CrossRef] [PubMed]
7. Barbinta-Patrascu, M.-E.; Iftimie, S.; Cazacu, N.; Stan, D.L.; Costas, A.; Balan, A.E.; Chilom, C.G. Bio-Entities Based on Albumin Nanoparticles and Biomimetic Cell Membranes: Design, Characterization and Biophysical Evaluation. *Coatings* **2023**, *13*, 671. [CrossRef]
8. Amighi, F.; Emam-Djomeh, Z.; Labbafi-Mazraeh-Shahi, M. Effect of different cross-linking agents on the preparation of bovine serum albumin nanoparticles. *J. Iran. Chem. Soc.* **2020**, *17*, 1223–1235. [CrossRef]
9. Imamura, K.; Ogawa, T.; Sakiyama, T.; Nakanishi, K. Effects of Types of Sugar on the Stabilization of Protein in the Dried State. *J. Pharm. Sci.* **2003**, *92*, 266–274. [CrossRef] [PubMed]
10. An, F.F.; Zhang, X.H. Strategies for preparing albumin-based nanoparticles for multifunctional bioimaging and drug delivery. *Theranostics* **2017**, *7*, 3667–3689. [CrossRef]
11. Zielińska, D.; Szawara-Nowak, D.; Zieliński, H. Determination of the antioxidant activity of rutin and its contribution to the antioxidant capacity of diversifed buckwheat origin material by updated analytical strategies. *Pol. J. Food Nutr. Sci.* **2010**, *60*, 315–321.
12. Pandey, P.; Khan, F.; Qari, H.A.; Oves, M. Rutin (Bioflavonoid) as Cell Signaling Pathway Modulator: Prospects in Treatment and Chemoprevention. *Pharmaceuticals* **2021**, *14*, 1069. [CrossRef] [PubMed]
13. Bonechi, C.; Donati, A.; Tamasi, G.; Leone, G.; Consumi, M.; Rossi, C.; Lamponi, S.; Magnani, A. Protective effect of quercetin and rutin encapsulated liposomes on induced oxidative stress. *Biophys. Chem.* **2018**, *233*, 55–63. [CrossRef]
14. Sengupta, P.; Sardar, P.S.; Roy, P.; Dasgupta, S.; Bose, A. Investigation on the interaction of Rutin with serum albumins: Insights from spectroscopic and molecular docking techniques. *J. Photochem. Photobiol. B* **2018**, *183*, 101–110. [CrossRef] [PubMed]

15. Sandu, N.; Chilom, C.G.; Popescu, A.I. Spectroscopic Insights on the Binding of Rutin to Bovine Serum Albumin. *Rom. J. Phys.* **2020**, *65*, 703.
16. Guruvayoorappan, C.; Kuttan, G. Rutin inhibits nitric oxide and tumor necrosis factor-alpha production in lipopolysaccharide and concanavalin-a stimulated macrophages. *Drug Metab. Drug Interact.* **2007**, *22*, 263–278. [CrossRef]
17. Wang, H.; Wang, L.; Guo, S.; Liu, Z.; Zhao, L.; Qiao, R.; Li, C. Rutin-Loaded Stimuli-Responsive Hydrogel for Anti-Inflammation. *ACS Appl. Mater. Interfaces* **2022**, *14*, 26327–26337. [CrossRef]
18. Matsuo, M.; Sasaki, N.; Saga, K.; Kaneko, T. Cytotoxicity of Flavonoids toward Cultured Normal Human Cells. *Biol. Pharm. Bull.* **2005**, *28*, 253–259. [CrossRef]
19. Abreu, A.C.; Serra, S.C.; Borges, A.; Saavedra, M.J.; Mcbain, A.J.; Salgado, A.J.; Simões, M. Combinatorial Activity of Flavonoids with Antibiotics Against Drug-Resistant *Staphylococcus aureus*. *Microb. Drug Resist.* **2015**, *21*, 600–609. [CrossRef]
20. Soobrattee, M.A.; Bahorun, T.; Aruoma, O.I. Chemopreventive actions of polyphenolic compounds in cancer. *BioFactors* **2006**, *27*, 19–35. [CrossRef]
21. Gong, G.; Qin, Y.; Huang, W.; Zhou, S.; Yang, X.; Li, D. Rutin inhibits hydrogen peroxide-induced apoptosis through regulating reactive oxygen species mediated mitochondrial dysfunction pathway in human umbilical vein endothelial cells. *Eur. J. Pharmacol.* **2010**, *628*, 27–35. [CrossRef]
22. Negahdari, R.; Bohlouli, S.; Sharifi, S.; Maleki Dizaj, S.; Rahbar Saadat, Y.; Khezri, K.; Jafari, S.; Ahmadian, E.; Gorbani Jahandizi, N.; Raeesi, S. Therapeutic benefits of rutin and its nanoformulations. *Phytother. Res.* **2021**, *35*, 1719–1738. [CrossRef]
23. Budiman, A.; Rusdin, A.; Aulifa, D.L. Current Techniques of Water Solubility Improvement for Antioxidant Compounds and Their Correlation with Its Activity: Molecular Pharmaceutics. *Antioxidants* **2023**, *12*, 378. [CrossRef]
24. Hornok, V. Serum Albumin Nanoparticles: Problems and Prospects. *Polymers* **2021**, *13*, 3759. [CrossRef]
25. Giri, T.K. Alginate Containing Nanoarchitectonics for Improved Cancer Therapy. In *Nanoarchitectonics for Smart Delivery and Drug Targeting*; William Andrew Publishing; Elsevier: Amsterdam, The Netherlands, 2016; pp. 565–588.
26. David, M.; Budziak-Wieczorek, I.; Karcz, D.; Florescu, M.; Matwijczuk, A. Insight into dual fluorescence effects induced by molecular aggregation occurring in membrane model systems containing 1,3,4-thiadiazole derivatives. *Eur. Biophys. J.* **2021**, *50*, 1083–1101. [CrossRef]
27. Pedrozo, R.C.; Antônio, E.; Khalil, N.M.; Mainardes, R.M. Bovine serum albumin–based nanoparticles containing the flavonoid rutin produced by nano spray drying. *Braz. J. Pharm. Sci.* **2020**, *56*, e17692. [CrossRef]
28. Kızılbey, K. Optimization of Rutin-Loaded PLGA Nanoparticles Synthesized by Single-Emulsion Solvent Evaporation Method. *ACS Omega* **2019**, *4*, 555–562. [CrossRef]
29. Rohiwal, S.S.; Tiwari, A.P.; Verma, G.; Pawar, S.H. Preparation and evaluation of bovine serum albumin nanoparticles for ex vivo colloidal stability in biological media. *Colloids Surf. A Physicochem. Eng. Asp.* **2015**, *480*, 28–37. [CrossRef]
30. Enache, T.A.; Oliveira-Brett, A.M. Phenol and para-substituted phenols electrochemical oxidation pathways. *J. Electroanal. Chem.* **2011**, *655*, 9–16. [CrossRef]
31. Sun, W.; Yang, M.; Li, Y.; Jiang, Q.; Liu, S.; Jiao, K. Electrochemical behavior and determination of rutin on a pyridinium-based ionic liquid modified carbon paste electrode. *J. Pharm. Biomed. Anal.* **2008**, *48*, 1326–1331. [CrossRef] [PubMed]
32. Naumowicz, M.; Figaszewski, Z.A. Pore formation in lipid bilayer membranes made of phosphatidylcholine and cholesterol followed by means of constant current. *Cell Biochem. Biophys.* **2013**, *66*, 109–119. [CrossRef] [PubMed]